Silicon (2022) 14:6847–6860
https://doi.org/10.1007/s12633-021-01430-8

ORIGINAL PAPER

Effect of Reinforcement Particles on Friction Stir Welded Joints with Scarf Configuration: an Approach to Achieve High Strength Joints

Durjyodhan Sethi[1] · Uttam Acharya[2] · Sanjeev Kumar[1] · Shashank Shekhar[3] · Barnik Saha Roy[1]

Received: 10 August 2021 / Accepted: 26 September 2021 / Published online: 19 October 2021

Abstract
The present research paper deals principally with the aim to achieve high strength through combined effect of incorporation of reinforcement particles in Friction stir scarf welded joints. The idea is implicated on AA6061-T6 plates with scarf angles of 60° and on different volume fraction (vol%) of reinforcement particles. A double pass FSW was performed using a taper threaded tool at a rotating speed (TRS) of 1100 rpm, a travel speed (TTS) of 2 mm/s, and a tool tilt angle (TTA) of 2°. The current study's goal is to investigate the macrostructure and microstructure development, as well as the joint's mechanical properties. The optical microscopy reveals fine, recrystallized and equiaxed grain in the nugget zone (NZ) due to the pinning effect of reinforcement particles. It has been observed through the scanning electron microscopy that higher grain refinement along with homogeneous distribution of SiC particles were achieved in multi-pass as compared to single pass. There is also strong bond formed between the aluminium matrix and the reinforcing particle. Moreover, it has been observed that when the vol% of reinforcement increases, the hardness and ultimate tensile strength (UTS) values improves while the % elongation decreases. The UTS has found to be increased by 12 % at 15 vol% of reinforcement. All tensile specimens failed outside the NZ with ductile fracture during tensile testing.

Keywords Friction stir welding · Scarf joint configuration · Reinforcing particle · Microstructure

1 Introduction

The sustainability of any engineering process depends on the continuous development of the existing process. For example, the friction stir welding (FSW) of modern engineering materials [1–3]. From the inception of FSW [4], a continuous development is going on to achieve more strong and stiff weld joints. It has been found that the improper selection of joint configuration, process parameter, and tool geometry cause a variety of defects in the butt joint. Some of the defects like hooking defect, incomplete root penetration, tunnel defect, joint line remnants, void formation, and kissing bonds are formed in butt joint configuration due difference in material flow around the periphery and axis of the tool. The research shows that the scarf joint has the potential to overcome this problem. The scarf joint configuration is new joint configuration in FSW, where the faying surface are inclined to the tool axis and hence serving higher faying surface area compared to the butt joint configuration [5]. Due to higher faying surface area, there is a substantial movement of material from one side of the plate to the other side and results in reduction of many defects and enhance the joint strength in FSW. The scarf joint configuration in FSW can have a significant effect on the joint strength due to the above mentioned contributing causes. Until now, there has been a dearth of research on the utilization of scarf joint configurations in FSW. An initial work by Goel et al. [6] reports the analysis of scarf configuration on AA6063 using an arbitrarily selected scarf angle of 26°. Although the analysis has presented a report on the effect of

✉ Durjyodhan Sethi
durjyodhan84@gmail.com

[1] Department of Mechanical Engineering, NIT Agartala, Agartala 799046, India

[2] Department of Mechanical Engineering, ASETK, Amity University Kolkata, Kolkata, India

[3] Department of Material Science and Engineering, IIT Kanpur, Kanpur 208016, India

scarf angle on microstructure and mechanical properties, no elaborate discussion on selecting an appropriate scarf angle based on optimum plunge depth, plate position and plate thickness is available. Recently, Sethi et al. [5] have proposed an equation that determines the scarf angle within the physical dimensions of the tool geometry and the plate for achieving a defect-free joint based on this underlying principle. As per their thorough study, the effect of various scarf angles considering the tool shoulder and pin geometry on the joint strength, they have concluded that joint efficiency improves from 72.5 % (butt joint) to 86 % with scarf angle of 60°. With the change in tool configuration and plate thickness, the scarf angle will also change for achieving desired strength and enhancement in mechanical property. In separate study Sethi et al. [7] investigate the impact of scarf joint configuration in casted composite plate. From the investigation they concluded that joint strength of the composite plate enhances remarkably with modified joint configuration.

Amongst the various reported possible ways of increasing the joint strength, infusing the reinforcing particles along the joint line is also a possible promising method [8]. Various reinforcement particles like Al_2O_3, TiC, Mg_2Si, B_4C, TiB_2, SiC etc. have been used for this purpose [9, 10]. Among the many reinforcement materials, SiC is an excellent candidate for reinforcing the Al matrix due to its superior properties in comparison to other reinforcement materials. SiC has many desirable properties, including high strength, hardness, high thermal shock resistance, excellent wear resistance, excellent chemical resistance, excellent corrosion resistance, low density, low thermal expansion, and high thermal conductivity, as well as good oxidation resistance and inexpensive [8, 9, 11]. According to Karakizis et al. [12] report on the influence of ceramic nanoparticles' reinforcement on FSW of AA6082-T6 alloy, it has been reported that the grain size decreases due to the pinning effect driven by the incorporation of nano particles. In addition to this, microhardness of the joint increases with addition of the TiC reinforcement. Sun et al. [13] have reported the impact of SiC particle on mechanical and microstructure properties of FSW of copper joint. They reported homogeneous distribution of SiC particle in the weld zone (WN) which results in increase in hardness and UTS after two welding passes. Bahrami et al. [14] have revealed that with the inclusion of the nano - SiC reinforcement particle, UTS and elongation percentage are getting enhanced by 31 % and 76.1 % respectively. From Karthikeyan et al. [15] finding on the influence of incorporation of SiC particle during FSW of AA6351 alloy, it has been found that with the SiC addition, the mechanical properties of the joints are getting enhanced as compared to the unreinforced one. The selection of the suitable vol% of the reinforcement is the most crucial thing is to increase the quality of the joint. It is found that vol% of the reinforcement affect the microstructure and strength of the joint [16–19]. According to Bahrami et al. [20] reported on the influence of SiC particle in FSWed AA7075 alloy, it is revealed that the mechanical strength of the joint increase with the incorporation of 20 vol% of SiC particles. Rathee et al. [11] study the effect of groove dimension on mechanical and microstructural properties of AA6063/SiC composites fabricate by FSP. They observed that groove width has strong effect on surface composite and maximum 40 vol% of reinforcement was successfully fabricated through FSP. As per the report of Abbasi et al. [21] on the impact of SiC reinforcement particle on mechanical and microstructure properties of AZ31 magnesium alloy, it has been observed that when SiC reinforcement particles are added, the grain size in NZ decreases and the joint strength is increases.

Many researchers [9–12, 22, 23] have also presented the effect of number of passes on the mechanical and microstructural property of FSW joint incorporation with ceramic reinforcement particle. Kumar et al. [19] evaluated the effect of SiC reinforcement vol% on microstructural and mechanical properties of FSWed joint of dissimilar aluminum alloy on the perspectives of number of passes. From their experiment they observed that the multi passes enhances the mechanical properties as compared to unreinforced alloys. Rathee et al. [11] examined the effect of SiC reinforcing particle size on the mechanical and microstructural characteristics of an AA5959/SiC composite fabricate through FSP. They determined from their analysis that significance enhancement of mechanical properties was obtained through multi pass FSP.

From the above discussion, it is pertinent to mention that the strength of the joints can be increased to a greater extent through the incorporation of reinforcement particles depending upon their nature and types. There can also be a supplementary augmentation in the strength if the geometry of the joint is also modified along with addition of reinforcements that have not been reported earlier. In this study, an attempt has been made to achieve a high strength (near to the base material) weld joint by using scarf configuration and infusing reinforcement particle. The use of high-strength reinforcement in the scarf joint arrangement is supposed to enhance the joint strength, which is found to be very significant in aerospace and defence applications. To support the study, macrostructure and microstructure, weld surface appearance, particles analysis, and mechanical properties of the joint were studied.

2 Materials and Methods

AA6061-T6 plates of dimensions of 150 mm × 65 mm × 6 mm were used for the current investigation. The descriptions of the workpiece are given in the Table 1. Based on tool geometry and dimensions, the optimum scarf angle without defect was proposed as 60° using the Eq. (1) and Eq. (2) [2].

Table 1 Description of the base material and tool material

Material used	AA6061-T6
Base plate dimension	150 mm × 65 mm × 6 mm
Chemical composition of base material (wt%)	Mg (1.2), Fe (0.75), Si (0.6), Cu (0.2), Mn (0.15), Cr (0.04), Al (Bal.)
Base material Mechanical property	UTS (MPa) — 310, YS (MPa) —276, elongation (%) — 18, hardness ($HV_{0.1}$) —107
Tool Material and Mechanical property	H13 tool steel, Hardness -58 HRC
Diameter of tool shoulder	18 mm
Bottom and top tool pin diameter	6 mm and 3 mm

$$\theta_1 = \tan^{-1}\left(\frac{h}{r_{pr} + r_{pt}}\right) \quad (1)$$

$$\theta_2 = \tan^{-1}\left(\frac{h}{r_s + r_{pt}}\right) \quad (2)$$

where

r_{pr} *and* r_{pt} are root and tip radius of pin, r_s is tool shoulder radius.

The scarf joint configuration with scarf angle of 60 ° was considered for the study as shown Fig. 1. The base material (BM) plate with required scarf angle as depicted in the Fig. 1 is machined using universal milling machine. A groove of width 2 mm and varying depth (as per volume fraction) is made using universal milling machine in the inclined region along the weld centre line. In order to obtain homogeneous reinforcement particle distribution, the grooves are made horizontally at the centre of plate thickness as shown in the Fig. 2(a). A plate without a groove was also used for the comparison purpose. In this experiment, SiC powder with an average particle size of 18 µm is employed. Figure 2(b) illustrates a SEM image of SiC particles.

The welding was conducted on a dedicated 3-TR FSW machine as shown in Fig. 3(a) that could deliver up to 30-kN of axial thrust on the tool. A taper threaded tool used in this experiment is shown in Fig. 3(b) (details listed in Table 1). The joining is performed at a constant machine parameter of

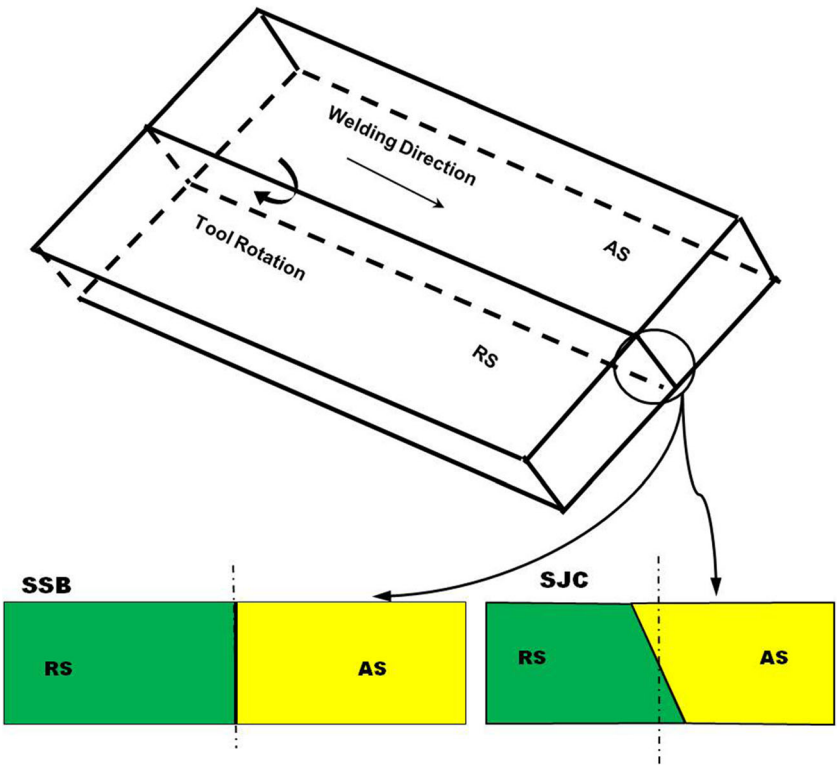

Fig. 1 Schematic representation of butt joint and scarf joint configuration

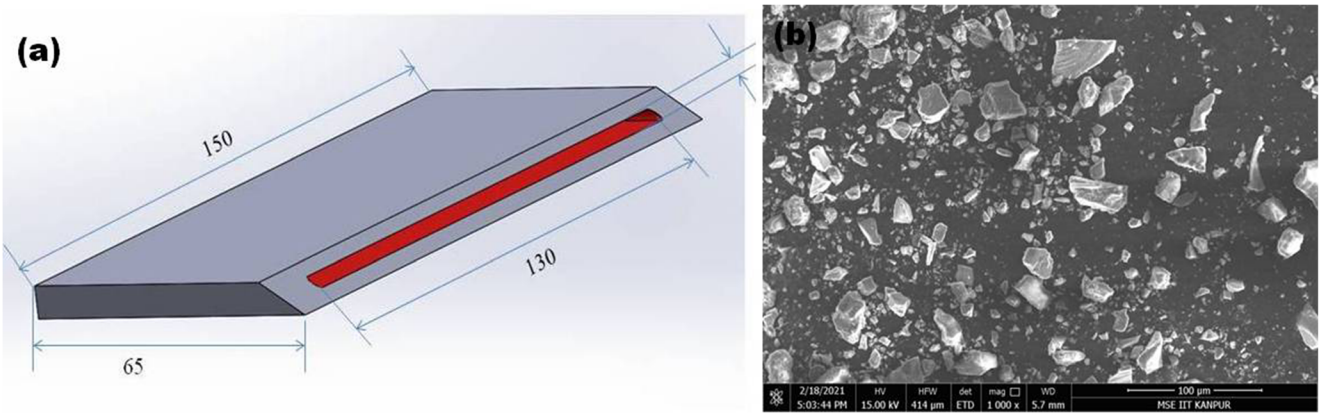

Fig. 2 (**a**) Workpiece with reinforcement groove, (**b**) SEM image of SiC particles

TRS, TTS and TTA (1100 rpm, 2 mm/s, and 2°) with varying vol% (0 %, 5 %, 10 %, and 15 %) of reinforcement. The vol% of SiC particles are calculated according to the expression given below-

$$\text{Volume fraction (Vf)} \frac{\text{area of grove}}{\text{projected area of tool pin}} \tag{3}$$

$$\text{Area of grove} = \text{grove width} \times \text{grove depth} \tag{4}$$

$$\text{Projected area of pin} = \text{pin diameter} \times \text{pin length} \tag{5}$$

To eliminate the influence of the thermal cycle observed in the earlier experiment, all the welding were done on different set of plates. Tensile test samples were made transverse to the welding direction, and specimens are measured using the ASTM-E8 specification standard with a strain rate of 1 mm/min. The macrostructure, microstructure, and hardness of the weld samples were determined by polishing them with emery paper grit sizes ranging from 150 to 2000, preceded by velvet cloth polishing with colloidal silica. For microstructure analysis, the specimens are dipping in Keller's reagent for 15-20 s after which the samples are cleaned with ethanol or water. A light optical microscope and a tungsten-scanning electron microscope (W-SEM) are used to examine the microstructure of the samples. According to ASTM E 112-12, the particle size of NZ is determined by using the linear intercept method. A load of 100 gf and a dwell time of 10 s are used to determine the Vickers microhardness value. The tensile fractured specimen is subjected to fractography analysis by using (W-SEM).

3 Results and Discussion

The purpose of this study is to demonstrate the influence of variation in the vol% of reinforcing particles on a friction stir scarf welded joint. As previously discussed by

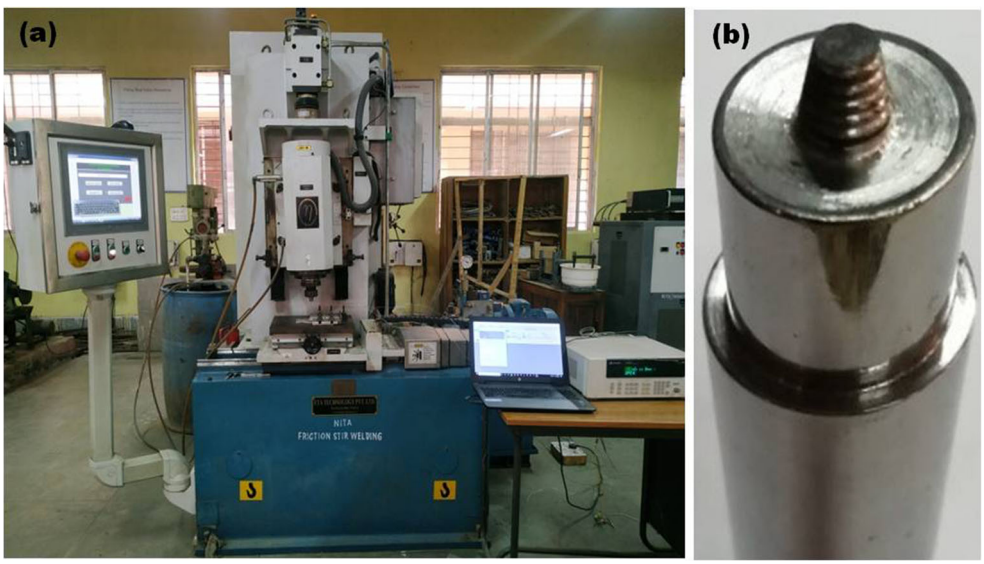

Fig. 3 (**a**) FSW setup, (**b**) Tool used during experiment

Sethi et al. [5], the joint strength in the scarf joint configuration is enhanced compared to the butt joint configuration. Thus, for all of the sections mentioned below, the comparison of scarf and butt joint configurations remains the same. The influence of reinforcing particle vol% on the welded structure will be evaluated initially visually, followed by an examination of the related macrostructure. Later on, the welding quality will be thoroughly examined using microstructural and EDS analysis. To establish an appropriate vol% of reinforcement particles for friction stirs scarf welded junction, the mechanical properties of the joint will be compared by using the hardness and tensile strength measurement.

3.1 Weld Surface and Quality Inspection

Figure 4 shows the weld surface quality for different vol% of the reinforcement. The selection of proper process parameters and the tool plunge depth helps in steady and uniform flow of the plasticized material for the whole length of the weld and results in defect free weld surface. A very smooth, identical and semi-circular crown can be seen without prominences or depressions on the weld surface. The amount of flash produce at 0 vol% of reinforcement is less as compared to the other (5 vol%, 10 vol% and 15 vol%) as second pass of FSW is carried out. It is also observed that, the amount of flash produced increased with the increase in vol% of the reinforcement. The explanation may be related to the heat generated under various parametric conditions which favours torque and force, resulting in material deformation. As the vol% of the reinforcement increases, the plasticized material's fluidity also increases and this helps the material to escape more easily from beneath the tool shoulder that results in excess flashing. To achieve a perfect friction stir zone, first a clear crown surface is achieved. The first stage in creating a friction stir zone with a clear surface is to have a faultless surface in the crown.

3.2 Macrostructural Characterization

Due to irregular material flow and a variety of intermixing mechanisms, it is challenging to obtain uniform reinforcement particle distribution in the welding zone of a single pass FSW. The current study uses two passes FSW approach to minimise asymmetry and improvement in the dispersion of reinforcement particles. Figure 5 shows the macrostructure of the FSW specimens for the first and second passes. It can be observed from Fig. 5(a) that the single FSW pass results in formation of void and non-homogeneous particle distribution. On the other side, no such observation can be seen from the macrostructure of the welded sample after second pass as shown in Fig. 5(b). This could be because of the two pass processed specimens having much more even distribution of particles than one pass processed specimen. Hamdollahzadeh et al. [22] and Sun et al. [13] also observed a better particle distribution in the second pass in their studies respectively.

The effect of vol% of SiC particles on the weld macrostructure of AA6061-T6 is shown in Fig. 6. The macrostructure is seemed to be symmetrical in all the cases. A basin-shaped nugget zone (NZ) has been developed at 5 % and 10 % vol. fraction of reinforcement whereas elliptical shaped is observed at 0 % and 15 %. The size and shape of stir zone (SZ) primarily depends on the processing parameters and tool geometry [22]. The area of weld nugget zone is evaluated using an image analyzing software. It is calculated as 35 mm^2, 37 mm^2, 33 mm^2 and 29 mm^2 at 0, 5 ,10 and 15 vol% of SiC respectively. It is observed that the NZ area decreases as the vol% of SiC particles increases. The area of the groove is increased to accommodate the higher vol% of the SiC particles. With an increase in SiC particles, the amount of aluminium in the parent matrix to be plasticized decreases. The flow stress to deform the plasticization material increases with the increase in the content of SiC particle. This may be due to non-deformable SiC particles that prevent the plasticized aluminum to flow freely. As a result, the SiC vol% increases whereas the NZ region decreases. Thangarasu et al. [16] and

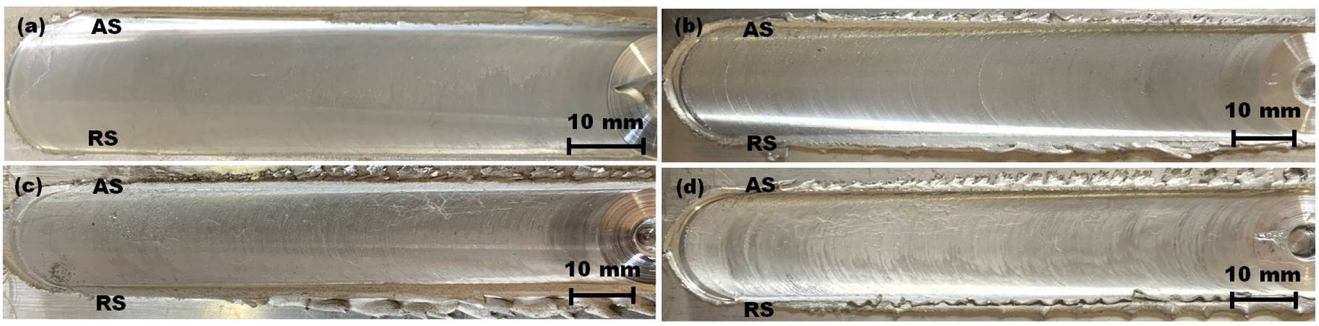

Fig. 4 Weld surface appearance (**a**) 0 vol%, (**b**) 5 vol%, (**c**) 10 vol%, (**d**) 15 vol%

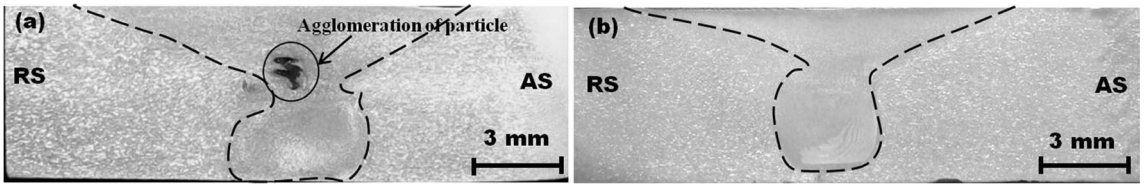

Fig. 5 Macrostructural images of (**a**) First pass, (**b**) Second pass

Rathee et al. [11] also observed decrease in NZ area with increase in groove area.

3.3 Microstructural Characterization

In FSW process, due to frictional heating and intense stirring effect of the FSW tool, recrystallized fine grains are generated in the NZ and elongated grains in thermo mechanically affected zone (TMAZ). The NZ and TMAZ of the first pass friction stir scarf welded joint with SiC particles are depicted in Fig. 7(a). An easily identifiable banded structure is observed in the NZ which is shown in the Fig. 7(b). The alternate particle rich and particle-free regions in the NZ are responsible for the development of banded microstructure. The band width formation is proportionate to the advancement of welding tool per revolution, which is also the primary cause of onion ring formation in NZ [24]. In the first pass of FSW, more prominent onion ring is visible in the NZ. This is attributed to the existence of particle-rich and particle-free areas in NZ, indicating an uneven distribution of reinforcing particles. To eliminate the aforementioned issue and to ensure uniform distribution of the reinforcing particles, a second pass FSW is performed [22, 25].

Figure 8 shows distribution of SiC reinforcement particle in NZ in (a) first and, (b) second FSW passes. The vol% and number of passes affect the dispersion of SiC particles in the NZ. It has been observed that particles are congregated at some places in first pass whereas in second pass they are distributed homogeneously. Additionally, SiC-rich regions are seen to be encircled by SiC-free zones, showing that the first pass of the FSW is insufficient for material mixing. The accumulation of SiC reinforcements in Fig. 8(a) is indicated by the dark zone. Due to second pass welding, the cluster size is reduced and uniform distribution is achieved throughout the NZ which is shown in Fig. 8(b).

The grain structure and distribution of SiC particles in the aluminium matrix is shown in Fig. 9. Different shapes and sizes of grains are generated in NZ at all the parameters as depicted in Fig. 9. Recrystallized fine equiaxed grains are observed in 0 vol% of the reinforcement. It is noticed that the grain size decreases with the increase in the vol% of the reinforcement. It is due to generation of the new nucleation sites by SiC reinforcement particles which act as hindrances against the grain growth and resulted in enhancing the dynamic recrystallization. This mechanism has been referred to as the pinning effect [22, 26]. Thangarasu et al. [16] and Hamdollahzadeh et al. [22] also observe the similar phenomenon with the incorporation of reinforcement particles. Since SiC particles act as an efficient grain refiner, the grain refinement can be due to their presence in the NZ. It can be seen that majority of SiC particles are present in the grain boundaries. No segregation of SiC particles have been observed in the grain boundary. The distribution of reinforcement particle in the NZ, determines the strength and property of the welding joint. With the increase in the vol% of the reinforcement particles, the particle density in the NZ increases with further increase in the pinning effect in the grain boundary. The strong pinning effect slows down the grain growth which aids in strengthening the mechanism by moving the dislocations along the grain boundaries. The grain size generated in NZ during FSW is calculated with the help of Zener–Holloman

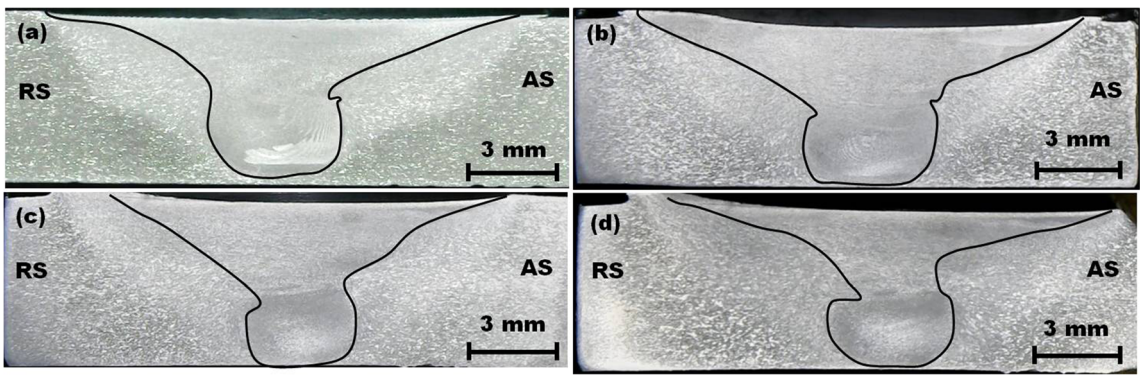

Fig. 6 Macrostructural images of NZ at (**a**) 0 % volume, (**b**) 5 % volume, (**c**) 10 % volume, (**d**) 15 % volume

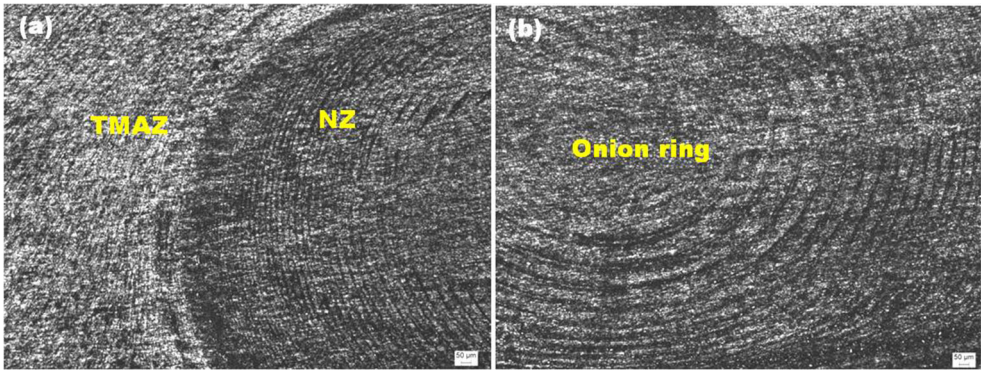

Fig. 7 Optical microstructural images at low magnification (**a**) Transition zone (**b**) NZ

parameter [19].

$$d_z = \frac{4r}{3v_f} \tag{6}$$

where, d_z is the Zener limiting grain size, the radius of the reinforcement particles is denoted by r and V_f is the vol% of the reinforcement particles. It has been observed from Eq. (6) that the grain size reduces as the vol% of reinforcing particle increases when the radius of the reinforcement particles remains constant.

The SEM image of SiC particles dispersion in different vol% of the reinforcement particles in the NZ is shown in Fig. 10. The particle dispersion is controlled by the flow of the material in the stir region. Reinforcement particles are evenly distributed for all the % vol. fraction of the reinforcement. The cluster size is minimized and dispersed uniformly throughout NZ due to the second pass welding. So, the dispersion of SiC particles in the NZ has been found to be somehow homogeneous. The density gradient prevents the particles from to move freely in the joint as it is formed in a solid state. The particles which move in the direction of the rotating tool in tangential motion. The reinforcement particle distribution nature is intra granular in the NZ. There is no evidence of any reaction product or micro pore at the interface between the SiC reinforcing particles and the aluminium matrix. The load bearing capacity of the joint is increased when the interface is clean in the AMC_S [16]. During the mechanical mixing, the plasticized aluminium matrix may be dispersed over the whole surface of the SiC particles preventing the development of micro pores.

Figure 11 shows the Energy Dispersive Spectroscopy (EDS) analysis of NZ at 15 vol% of reinforcement. Spot EDS analysis is carried out in spot 1 and spot 2 to determine the elemental composition of the NZ in wt%, as shown in Fig. 11. Spectrum 1 depicts the key constituents of the AA6061 alloy, while spectrum 2 depicts the presence of silicon and carbon particles as a matrix reinforcing element. As a result of the EDS examination, it can be concluded that NZ is made up of AA6061 alloy and SiC particles. The existence of the matrix and reinforcement phase's probable elemental composition is confirmed by this study.

3.4 Particle Size Analysis

This section systematically analyzes the quantity of dispersed reinforcement particles and size in the welding zone. Using Image-J software, the particle size is calculated for all images of similar area, scale, and magnification, and then distribution plots of particle size vs. counts are created for comparison. To

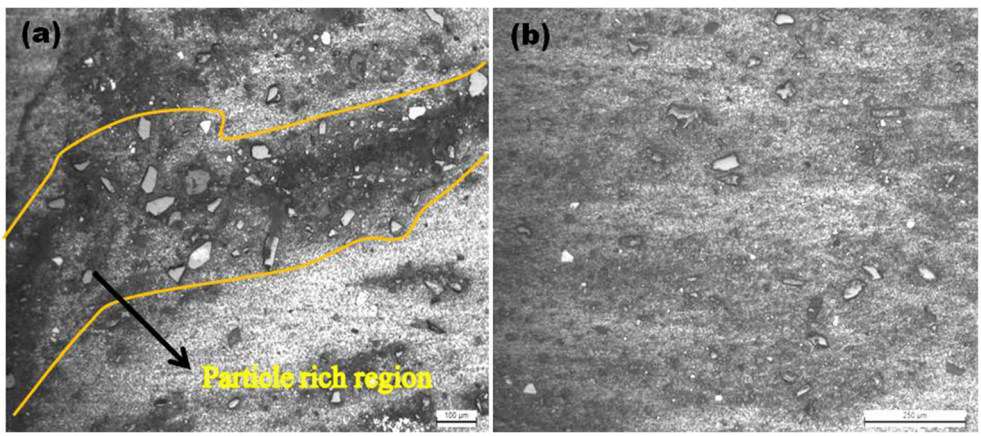

Fig. 8 Microstructural images (**a**) First pass FSW (**b**) Second pass FSW

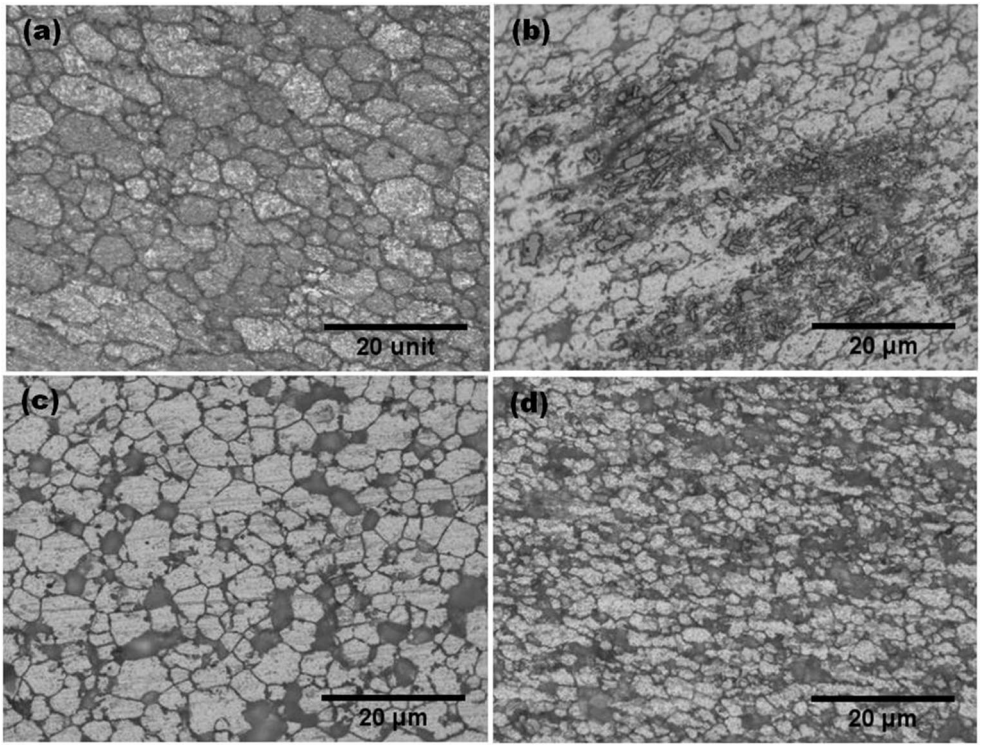

Fig. 9 Optical microstructural images (grain focused) of NZ at (**a**) 0 vol%, (**b**) 5 vol%, (**c**) 10 vol% (**d**) 15 vol%

confirm the validity of the analysis, three SEM pictures with identical resolution are taken from a given zone, and the plot is generated using the averages of each particle size observed throughout all three pictures. The study revealed that the smallest particle is 1 µm and the biggest particle size is 15 µm. To make the study easier, particles size larger than 8 µm are treated as coarse particles, whereas particles size smaller than 8 µm are treated as fine particle. Figure 12

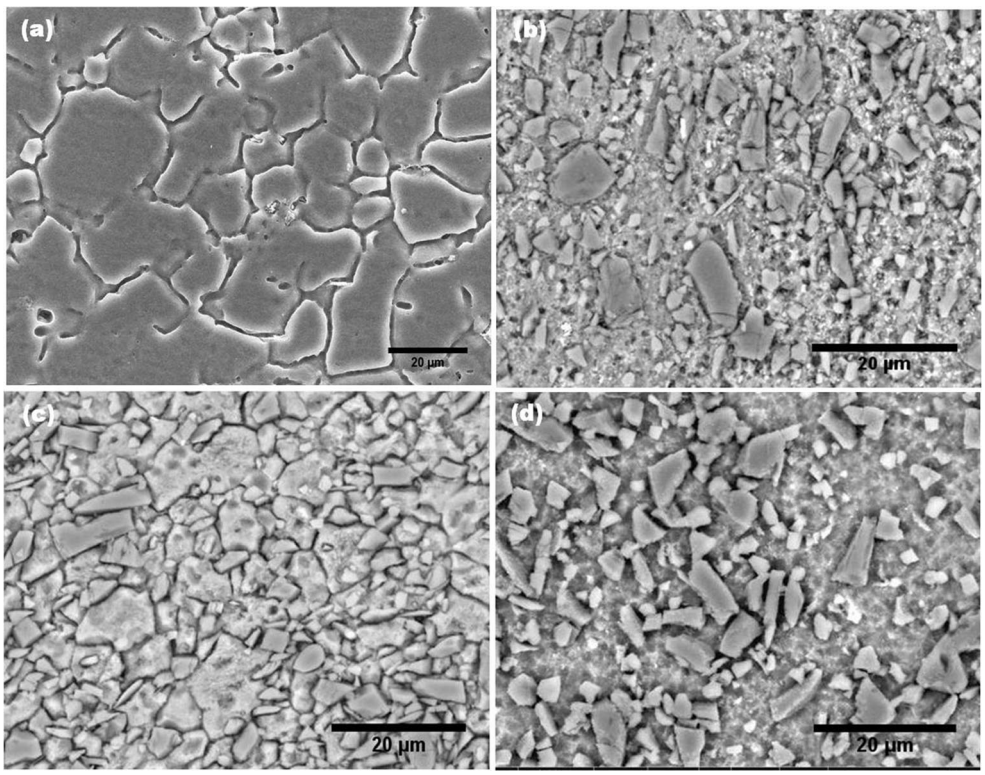

Fig. 10 SEM microstructural images of NZ at (**a**) 0 vol%, (**b**) 5 vol%, (**c**) 10 vol%, (**d**) 15 vol%

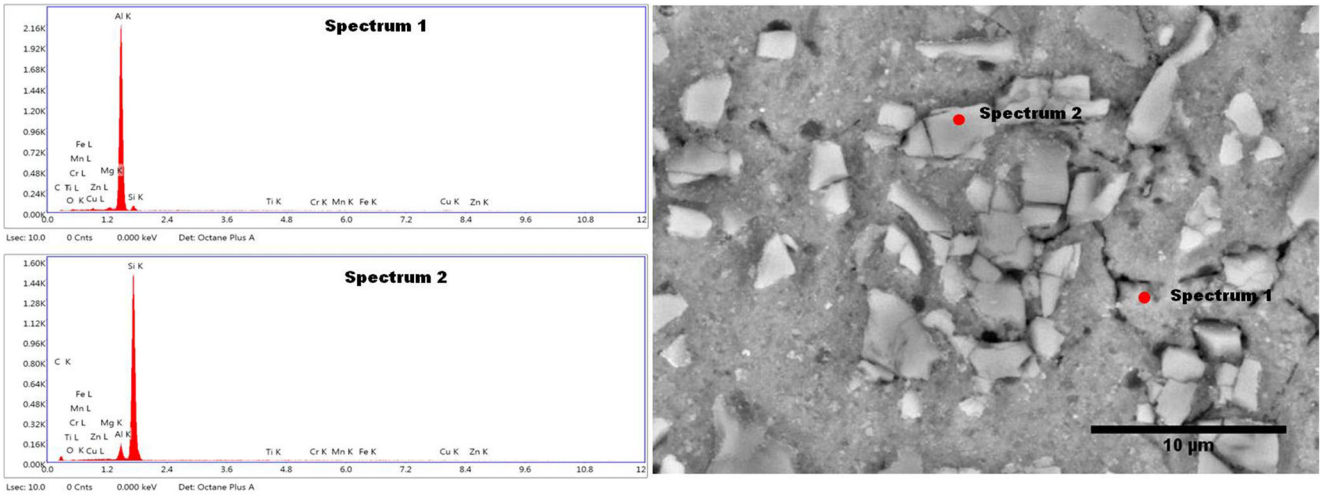

Element	C	O	Mg	Al	Si	Ti	Cr	Mn	Fe	Cu	Zn
Spectrum 1 (Wt.%)	0.19	1.06	1.32	93.41	0.42	0.32	0.21	0.25	0.21	2.34	0.27
Spectrum 2 (Wt.%)	9.25	0.26	0.43	17.61	70.26	0.39	0.26	0.21	0.31	0.57	0.45

Fig. 11 EDS analysis of friction stir scarf welded joint

demonstrates that the number of particles increases from 5 vol% to 15 vol% of the reinforcement particles. It may be seen in Fig. 12 that; larger counts of a coarse size particle are present at 15 vol% of the reinforcement compared to the rest of the parameter. The remaining plots in the graph indicate the existence of smaller particles (less than 8 m) in the microstructure. Additionally, it is found that the number and size of reinforcement particles varied with the vol% of reinforcement.

3.5 Effect of Reinforcement Particles on Tensile Strength

The overall effect of vol% of reinforcement on the weld zone is investigated from tensile strength analysis. Tensile values can be increased or decreased by defining the vol% of reinforcement and the grain size of the weld zone. Three specimens have been examined in each reinforcement condition and the average values are reported in Fig. 13. Several aspects affecting the mechanical characteristics of reinforced friction stir scarf welded joint specimens, including interactions between matrix and reinforcement particle under various process conditions, dislocation density, and grain size [10]. The reinforcement particles, as previously mentioned, have a major effect on the strength of welding joint. An increased SiC particle content in the weld joint enhances the joint strength whereas reducing its ductility. Chen et al. [1] demonstrate the strength of the composite increase with addition of the reinforcement particles. According to Orowan–Ashby strengthening mechanism [19], yield strength increases with increase in vol% of the reinforcement if there is no agglomeration in NZ which is represented in Eq. (7).

$$\sigma_{Orowan} = \frac{0.13 G_m b}{\lambda} ln \frac{r}{b} \tag{7}$$

where.

G_m is "matrix material's shear modulus", b is "burgers vector", r is "reinforcement particles' radius", and λ is "mean interparticle spacing". λ value for different vol.% of the reinforcement particles can be calculated using the Eq. (8)

$$\lambda = d_p \left[\left(\frac{1}{2v_p} \right)^{\frac{1}{3}} - 1 \right] \tag{8}$$

where

d_p is "diameter of SiC particles", and v_p is "volume fraction of the reinforcement".

From the Eq. (7) and Eq. (8), it has been observed that yield strength increases with increase the vol% of the reinforcement particle keeping other parameter constant. It is also a known fact that grain size decreases with increase in the vol% of reinforcement. It is due to pinning effect of grain boundary and grain refining; new nucleation site will develop which suppress the grain growth. Decrease in grain size enhance the mechanical property of the joint. This phenomenon may be explained by the Hall–Petch relationship described in Eq. (9), which states that UTS increases as grain size decreases [27].

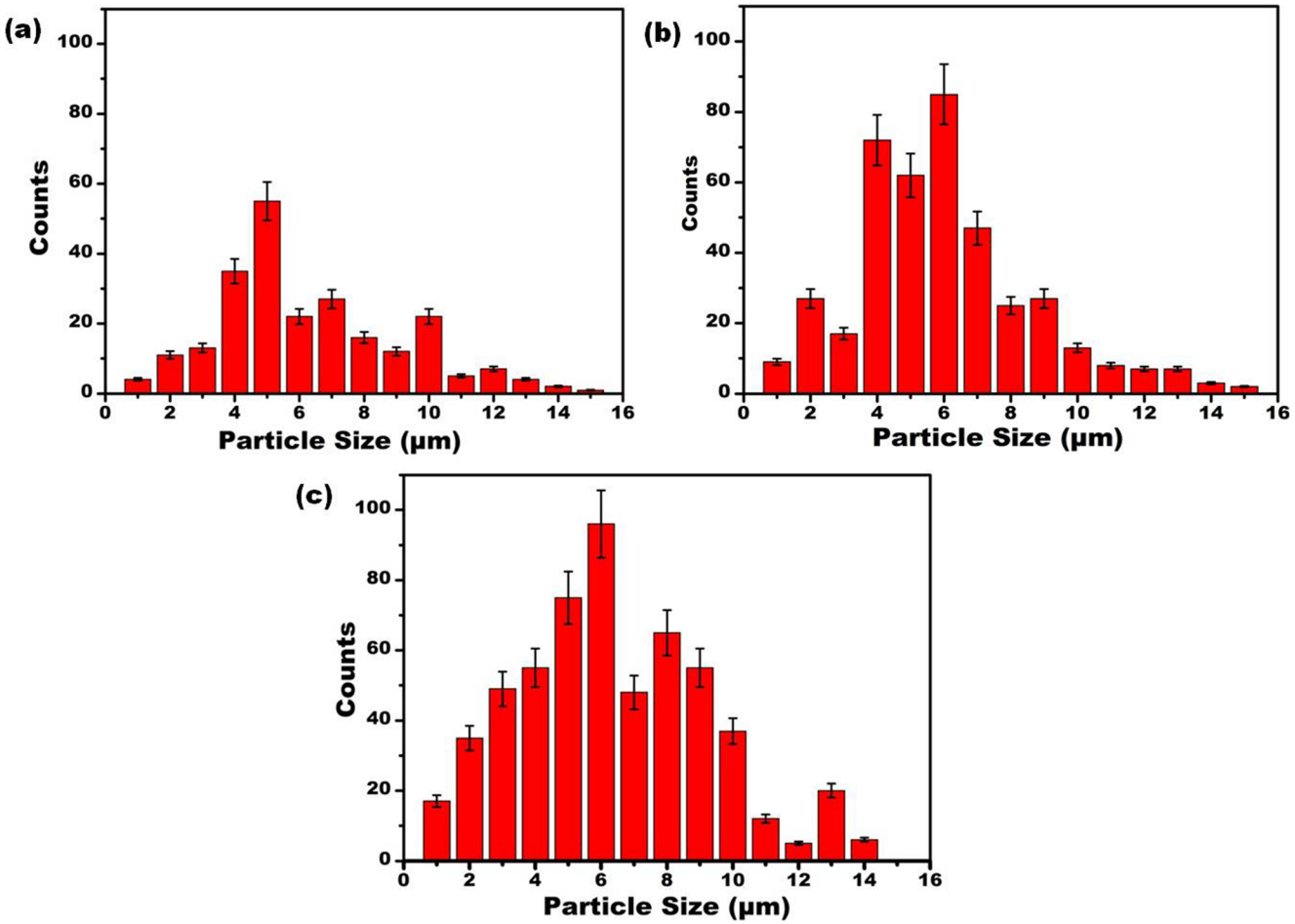

Fig. 12 Particle size distribution of (**a**) 5 vol% (**b**) 10 vol% (**c**) 15 vol% of reinforcement

$$\sigma_y = \sigma_0 + \frac{k}{\sqrt{D}} \tag{9}$$

where σ_y is "yield stress", σ_0 is "friction stress", K is "strengthening coefficient", and D is "average grain size diameter". Due to the smaller and more refined structure of SiC-included specimens, UTS was greater than in SiC-free specimens (0 % vol.). So, the strength of the welded joints increased with increase the vol.% of SiC reinforcement. It may be due to combine effect of above mention mechanism. Additionally, as illustrated in Fig. 13, % elongation decreases as the vol.% of the reinforcement particle increases. Increase in concentration of hard ceramic reinforcement particles can be attributed for the decrease in elongation. Figure 13 compares the UTS, % elongation, and 0.2 % Yield strength of different vol.% of welded specimens (5 %, 10 % and 15 %)

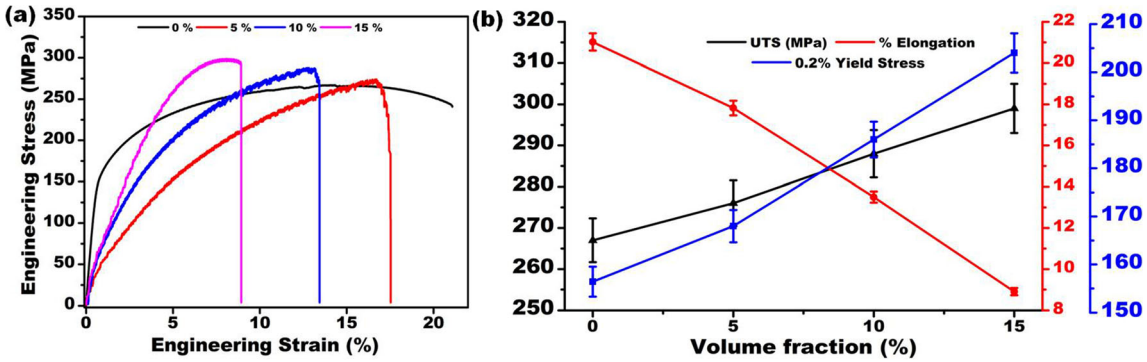

Fig. 13 Effect of vol% of reinforcement on (**a**) Engineering stress strain, (**b**) UTS, yield stress and elongation

to the unreinforced specimen (0 %). It has been observed from Fig. 13 that UTS values increases from 267 MPa (0 %) to 299 MPa (15 %), yield strength increases from157 MPa (0 vol.%) to 204 MPa (15 vol.%) whereas % elongation reduces from 21 % (0 vol.%) to 8.9 % (15 vol.%).

3.6 Effect of Reinforcement on Microhardness

Vickers microhardness is used to determine the microhardness variation throughout the midsection of the sample and perpendicular to the welding direction. The microhardness of the BM is approximately 107 $HV_{0.1}$ on average. The horizontal variation of microhardness along the central plane of NZ is depicted in Fig. 14. It is observed that heat input, grain size, particle content and dislocation density affect the microhardness of FSWed specimens reinforced with SiC particles [9]. The well-known Hall–Petch correlation states that decreasing particle size results in enhanced the hardness values [5]. Furthermore, because of the unequal thermal expansion coefficients of the matrix and reinforcing particle, dislocations are formed, resulting in increased hardness. Reinforcing particles appears to have a dual-action on hardness of the welded joint. The first is due to the hardness of SiC particles, and the second is due to the particles' impact on grain boundary pinning. It has been observed from Fig. 14(a) that microhardness value in AS is slightly lower than the RS, as the amount of heat generated AS is usually higher than RS. Strain rate inside the stir zone, different microstructural characteristics, and grain orientation within the NZ, all are contributed to microhardness variation in the stir zone, as a result, there is some anisotropy in the microhardness distribution over the stir zone's centre. Furthermore, the presence of SiC free and SiC rich regions can cause fluctuations in the microhardness profile. The addition of the hard reinforcement particles increased the hardness of the FSWed-joints, as shown in Fig. 14. The pinning effect is partly responsible for the increased hardness property of the NZ. As a result, grain recrystallization improved, resulting in a higher hardness property [26]. Hardness value increase from 0 vol% to 15 vol% of the reinforcement. This may be attributed due to an increase in the vol% of the hard ceramic particles. Also, as the grain size decrease with increase in vol% of the reinforcement. Thus, according to the Hall-Petch relationship, microhardness increases as the vol% of reinforcement increases. Figure 14(b) represent the variation of different zone average hardness with vol% of the reinforcement. It is noted that the hardness value of all the zone increases with increase in vol% of the SiC particles. The average hardness value of NZ increases from 87 $HV_{0.1}$ (0 vol%) to 119 $HV_{0.1}$ (15 vol%). Also, the hardness achieve in NZ is higher compare to the other zone (5 vol%, 10 vol% and 15 vol%). This due to presence of hard ceramic particles and small recrystallized grains in NZ compared to other zone.

4 Fractography Analysis

The fractographic investigations of the broken tensile specimens are shown in Fig. 15. To determine the location and mode of failure for all samples, the combined effect of heat input, grain size, hardness, and particle size must be thoroughly investigated. From the Fig. 15, it has been observed that for all the samples, fracture failure takes place outside the NZ preferably within the TMAZ during tensile testing. The specimen with 0 vol% and 5 vol% of the reinforcement failed in AS whereas specimens with 10 vol% and 15 vol% failed in RS during tensile test. Also, it has been observed that all the tensile sample fail in TMAZ. This may be attributed to the lowest hardness and strength in TMAZ compared to other region. As the TMAZ with coarse grains has lower hardness, the failure take place preferably in low strength region. The

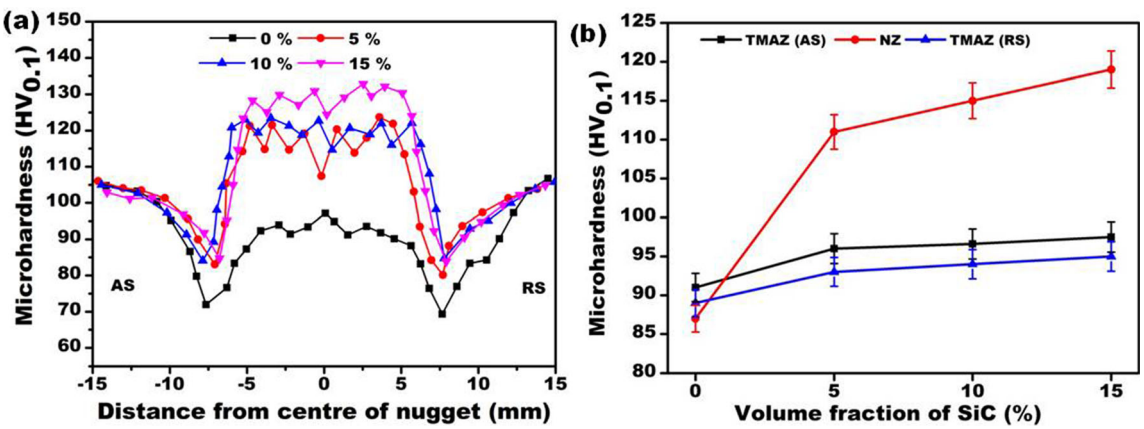

Fig. 14 Variation of microhardness with vol% of reinforcement

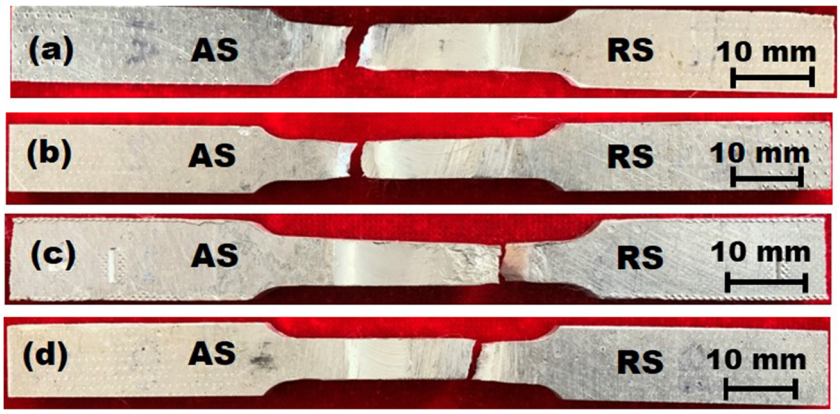

Fig. 15 Location of Fracture surface (**a**) 0 vol%, (**b**) 5 vol%, (**c**) 10 vol%, (**d**) 15 vol%

tensile fracture outside the NZ indicates a well-bonded interaction between the ceramic reinforcement particles and the aluminum matrix. Hamdollahzadeh et al. [22] also reported the fracture take place outside the NZ due to good bonding between reinforcement particles and aluminium matrix. The ability of load transfer from matrix to reinforcing particles determines the strength of the welding joint. So, it is highly dependent on achieving good interfacial bonding between ceramic reinforcement and aluminum matrix. Also due to poor interfacial bonding between the reinforcement and the aluminium matrix cause early failure of the joint before any load transfer, as a result joint strength decrease. So, the failure take place outside the NZ when, there is no pore and misalignment between reinforcement particles and aluminium matrix. The fracture occurred in the TMAZ of either AS or RS, suggesting that SiC particle was distributed uniformly and have a strong interfacial bonding with the aluminium alloy matrix at the NZ. So, the NZ strength is high compare to the other region. Also, the good bonding between the matrix and reinforcement is one of the reasons for fracturing outside the NZ. Bahrami et al. [20] also reported the failure of tensile specimen in TMAZ.

SEM micrographs of fractured surfaces in various vol% of the reinforcement are shown in Fig. 16. It can be concluded that specimens with 0 vol% of reinforcement have a large and deep dimple on the fracture surface. The existence of large and deep dimples on the tensile fracture surface indicating ductile mode of fracture [25]. Also, presence of large and deep

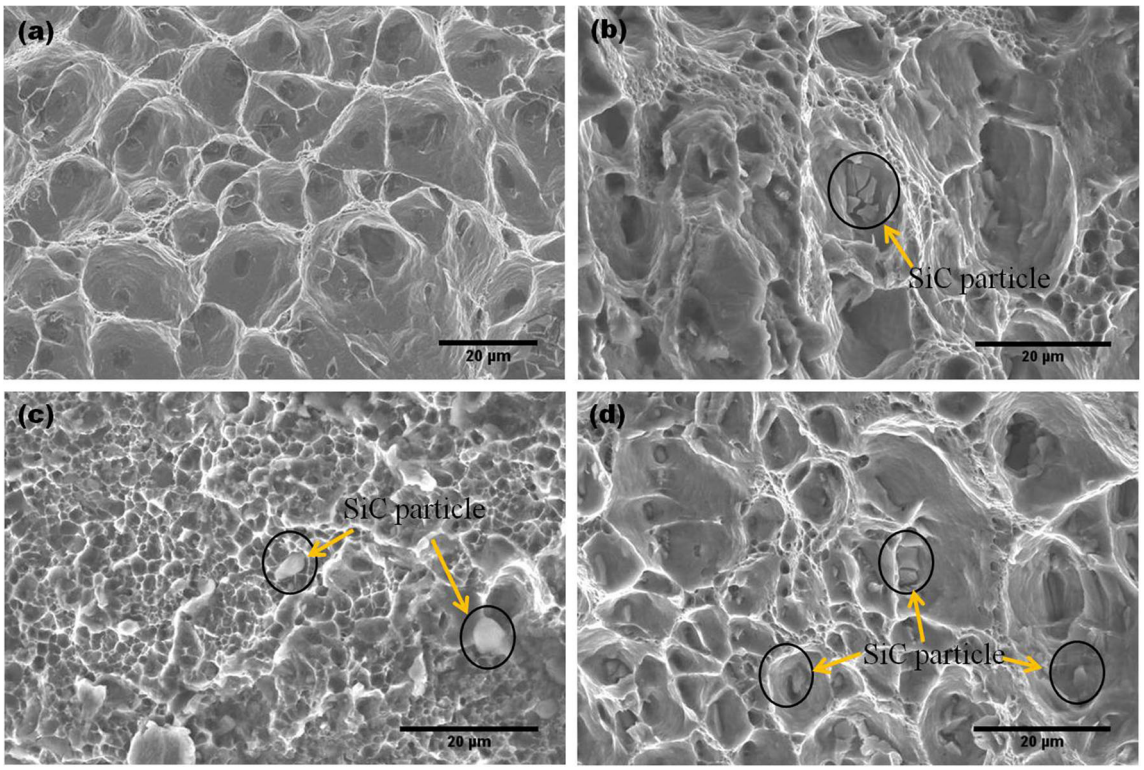

Fig. 16 Fracture surface with vol % reinforcement

dimples as well as small dimples on the tensile surface of 5 vol% of reinforcement indicate the ductile mode of failure. Mohammadzadeh et al. [22] also confirm the ductile mode of failure by the presence of as small dimples along with large and deep dimples. This is due to the specimen's smaller grain size, which provides greater resistance to fracture. As a result, the specimen failed on the advancing side of the TMAZ zone, where the hardness was lower. Presence of small dimple and large dimple (honey comb dimple) on the fracture surfaces indicate ductile mode of fracture, which is shown in 10 vol% of the reinforcement. Srivastava et al. [28] and Sabari et al. [29] also demonstrate the presence of small and large dimple indicate the ductile mode of failure. It has been observed that different size dimples along with void are present on the fracture surface of 15 vol% of the reinforcement, which indicate the ductile mode of fracture. Barmouz et al. [30] also describe the ductile mode of fracture due to ppresence of dimples and void characteristic on the fracture surfaces. It also seen that SiC particles are present on all fracture surfaces except those with a of 0 vol% reinforcing particles. The matrix's low strength resulted in cracking and the formation of several dimples on the fracture surface. The matrix's high strength increases the probability of SiC particle fracturing [31].

5 Conclusions

In this investigation different vol% of SiC particle (0 %, 5 %,10 % and 15 %) are incorporated between two adjoining surfaces of AA6061-T6 scarf joint configuration. On subsequent examination of the welded sample's macrostructure, microstructure and mechanical properties, the following conclusions are obtained.

- The second pass FSW in the NZ resulted in fine and equiaxed recrystallized grains, as well as SiC particle breakage and uniform dispersion.
- The macrostructure study revealed that there are no visible defects on the weld surface.
- In NZ, fine recrystallized grains are generated, and grain size decreases as the vol% of reinforcement increases.
- When the vol% of SiC particles is increased from 0 % to 15 %, the UTS also increases from 267 MPa to 299 MPa.
- NZ's average microhardness value increased from 87 $HV_{0.1}$ (0 vol%) to 119 $HV_{0.1}$ (15 vol%).
- For all parameters, fracture occurs outside the NZ and is characterized by a ductile failure mode.

Acknowledgements The first author wishes to thank the Ministry of Human Resource Development of India for giving funding in the form of a fellowship. The authors would like to thank the MSE department at IIT Kanpur (specifically Mrs. Samata Samal for microscopic imaging analysis) for their cooperation and smooth testing.

Author Contributions Durjyodhan Sethi: Conceptualization, Writing - original draft, Investigation. Uttam Acharya: Formal analysis, Methodology. Sanjeev Kumar: Resources, Visualization. Shashank Shekhar: review & editing, Barnik Saha Roy: final review & editing.

Data Availability The authors confirm that the data supporting the findings of this study are available within the article.

Declarations

Conflict of Interest The authors declare that they have no known competing financial interests.

Not Applicable.

Ethics Approval Not Applicable.

Consent for Publication Consent was obtained from all the authors for the publication of this manuscript.

Consent to Participate Not Applicable.

References

1. Chen XG, Da Silva M, Gougeon P, St-Georges L (2009) Microstructure and mechanical properties of friction stir welded AA6063–B4C metal matrix composites. Mater Sci Eng A 518(1-2):174–184
2. Yuvanarasimman P, Malayalamurthi R (2018) Studies on fractures of friction stir welded Al matrix SiC-B 4 C reinforced metal composites. Silicon 10(4):1375–1383
3. Ali KA, Mohanavel V, Ravichandran M, Vendan SA, Sathish T, Karthick A (2021) Microstructure and mechanical properties of friction stir welded SiC/TiB 2 reinforced aluminum hybrid composites. Silicon :1–11
4. Sachinkumar, Narendranath S, Chakradhar D (2019) Microstructure, hardness and tensile properties of friction stir welded aluminum matrix composite reinforced with SiC and fly ash. Silicon 11:2557–2565. https://doi.org/10.1007/s12633-018-0044-5
5. Sethi D, Acharya U, Shekhar S, Roy BS (2021) Applicability of unique scarf joint configuration in friction stir welding of AA6061-T6: Analysis of torque, force, microstructure and mechanical properties. Defence Technology. https://doi.org/10.1016/j.dt.2021.03.010
6. Goel P, Siddiquee AN, Khan NZ, Hussain MA, Khan ZA, Abidi MH, Al-Ahmari A (2018) Investigation on the effect of tool pin profiles on mechanical and microstructural properties of friction stir butt and scarf welded aluminium alloy 6063. Metals 8(1):74
7. Sethi D, Kumar S, Shekhar S, Roy BS (2021) Friction stir welding of AA7075-T6/TiB2 in situ cast composites plates using scarf joint configuration. Adv Mater Process Technol 1–13. https://doi.org/10.1080/2374068X.2021.1959092
8. Srivastava M, Rathee S (2021) A Study on the effect of incorporation of SiC particles during friction stir welding of Al 5059 alloy. Silicon 13(7):2209–2219. https://doi.org/10.1007/s12633-020-00722-9
9. Jamalian HM, Ramezani H, Ghobadi H, Ansari M, Yari S, Givi MKB (2016) Processing–structure–property correlation in nano-

SiC-reinforced friction stir welded aluminum joints. J Manuf Process 21:180–189
10. Dinaharan I, Murugan N (2012) Effect of friction stir welding on microstructure, mechanical and wear properties of AA6061/ZrB2 in situ cast composites. Mater Sci Eng A 543:257–266
11. Rathee S, Maheshwari S, Siddiquee AN, Srivastava M (2019) Investigating the effects of SiC particle sizes on microstructural andmechanical properties of AA5059/SiC surface composites during multi-passFSP. Silicon 11(2):797–805
12. Karakizis PN, Pantelis DI, Fourlaris G, Tsakiridis P (2018) Effect of SiC and TiC nanoparticle reinforcement on the microstructure, microhardness, and tensile performance of AA6082-T6 friction stir welds. Int J Adv Manuf Technol 95(9):3823–3837
13. Sun YF, Fujii H (2011) The effect of SiC particles on the microstructure and mechanical properties of friction stir welded pure copper joints. Mater Sci Eng A 528(16-17):5470–5475
14. Bahrami M, Dehghani K, Givi MKB (2014) A novel approach to develop aluminum matrix nano-composite employing friction stir welding technique. Mater Des 53:217–225
15. Karthikeyan P, Mahadevan K (2015) Investigation on the effects of SiC particle addition in the weld zone during friction stir welding of Al 6351 alloy. Int J Adv Manuf Technol 80(9):1919–1926
16. Thangarasu A, Murugan N, Dinaharan I, Vijay SJ (2015) Synthesis and characterization of titanium carbide particulate reinforced AA6082 aluminium alloy composites via friction stir processing. Arch Civ Mech Eng 15(2):324–334
17. Suresh S, Venkatesan K, Natarajan E (2018) Influence of SiC nanoparticle reinforcement on FSS welded 6061-T6 aluminum alloy. J Nanomater 2018. https://doi.org/10.1155/2018/7031867
18. Sahraeinejad S, Izadi H, Haghshenas M, Gerlich AP (2015) Fabrication of metal matrix composites by friction stir processing with different particles and processing parameters. Mater Sci Eng A 626:505–513
19. Kumar KSA, Murigendrappa SM, Kumar H (2019) Experimental investigation on effects of varying volume fractions of SiC nanoparticle reinforcement on microstructure and mechanical properties in friction-stir-welded dissimilar joints of AA2024-T351 and AA7075-T651. J Mater Res 34(7):1229–1247
20. Bahrami M, Helmi N, Dehghani K, Givi MKB (2014) Exploring the effects of SiC reinforcement incorporation on mechanical properties of friction stir welded 7075 aluminum alloy: fatigue life, impact energy, tensile strength. Mater Sci Eng A 595:173–178
21. Abbasi M, Abdollahzadeh A, Bagheri B, Omidvar H (2015) The effect of SiC particle addition during FSW on microstructure and mechanical properties of AZ31 magnesium alloy. J Mater Eng Perform 24(12):5037–5045
22. Hamdollahzadeh A, Bahrami M, Nikoo MF, Yusefi A, Givi MB, Parvin N (2015) Microstructure evolutions and mechanical properties of nano-SiC-fortified AA7075 friction stir weldment: The role of second pass processing. J Manuf Process 20:367–373
23. El-Rayes MM, El-Danaf EA (2012) The influence of multi-pass friction stir processing on the microstructural and mechanical properties of Aluminum Alloy 6082. J Mater Process Technol 212(5): 1157–1168
24. Sutton MA, Yang B, Reynolds AP, Taylor R (2002) Microstructural studies of friction stir welds in 2024-T3 aluminum. Mater Sci Eng A 323(1-2):160–166
25. Asadi P, Givi MB, Abrinia K, Taherishargh M, Salekrostam R (2011) Effects of SiC particle size and process parameters on the microstructure and hardness of AZ91/SiC composite layer fabricated by FSP. J Mater Eng Perform 20(9):1554–1562
26. Abioye TE, Zuhailawati H, Anasyida AS, Yahaya SA, Dhindaw BK (2019) Investigation of the microstructure, mechanical and wear properties of AA6061-T6 friction stir weldments with different particulate reinforcements addition. J Mater Res Technol 8(5): 3917–3928
27. Kumar S, Acharya U, Sethi D, Medhi T, Roy BS, Saha SC (2020) Effect of traverse speed on microstructure and mechanical properties of friction-stir-welded third-generation Al–Li alloy. J Braz Soc Mech Sci Eng 42(8):1–13
28. Srivastava M, Rathee S, Siddiquee AN, Maheshwari S (2019) Investigation on the effects of silicon carbide and cooling medium during multi-pass FSP of Al-Mg/SiC surface composites. Silicon 11(4):2149–2157
29. Sabari SS, Malarvizhi S, Balasubramanian V, Reddy GM (2016) Experimental and numerical investigation on under-water friction stir welding of armour grade AA2519-T87aluminium alloy. Def Technol 12(4):324–333
30. Barmouz M, Asadi P, Givi MB, Taherishargh M (2011) Investigation of mechanical properties of Cu/SiC composite fabricated by FSP: Effect of SiC particles' size and volume fraction. Mater Sci Eng A 528(3):1740–1749
31. Wang D, Xiao BL, Wang QZ, Ma ZY (2013) Friction stir welding of SiCp/2009Al composite plate. Mater Des 47:243–247